

Assessing the impact of various wind forcing on INCOIS-GODAS simulated ocean currents in the equatorial Indian Ocean

Sanikommu Sivareddy¹ · Muthalagu Ravichandran¹ ·
Madathil Sivasankaran Girishkumar¹ · Koneru Venkata Siva Rama Prasad²

Received: 30 September 2014 / Accepted: 19 August 2015 / Published online: 2 September 2015
© Springer-Verlag Berlin Heidelberg 2015

Abstract The Global Ocean Data Assimilation System configured at Indian National Centre for Ocean Information Services (INCOIS-GODAS) has been forced with satellite-based QuikSCAT gridded winds (QSCAT) to obtain accurate operational ocean analysis, particularly ocean currents, as compared to the default National Centers for Environmental Prediction-Reanalysis 2 (NCEP-R2) wind forcing in the tropical Indian Ocean (TIO). However, after termination of QuikSCAT mission in November 2009, an alternate wind forcing was required for providing operational ocean analysis. The present study examines the suitability of an Advanced Scatterometer (ASCAT)-based daily gridded wind product (DASCAT) for the INCOIS-GODAS. Experiments were performed by forcing INCOIS-GODAS with three different momentum fluxes derived from QSCAT, DASCAT, and NCEP-R2 wind products. Simulated ocean currents from these experiments are validated with respect to in situ current measurements from Research Moored Array for African-Asian-Australian Monsoon Analysis and Prediction (RAMA) buoys. Results suggested that the quality of simulated ocean currents from the daily DASCAT forcing is on par with the QSCAT forcing in the TIO, except for the equatorial Indian Ocean (EIO). Although QSCAT-forced current simulations are slightly better than DASCAT-forced simulations, both

QSCAT and DASCAT provide a much better result than NCEP-R2. Our analysis shows that the better simulations of currents over the EIO, with the QSCAT forcing compared to DASCAT forcing, can be attributed to the smoothing of the wind field in the DASCAT compared to QSCAT. The impact of the error in the DASCAT on ocean current analysis is, however, limited to local scales and upper 100 m of water column only. Thus, our study demonstrated that, in the absence of QSCAT, DASCAT is a better alternative for INCOIS-GODAS ocean analysis than the NCEP-R2.

Keywords Wind evaluation · ASCAT · Ocean models · INCOIS-GODAS · Wind error impact · Equatorial Indian Ocean

1 Introduction

The demand for high-quality, dynamically consistent ocean analysis product both in spatial and temporal scales has increased significantly in the recent times. Such dynamically consistent ocean analysis products are very important components of coupled ocean-atmospheric models used for operational weather forecast. They are also useful for the studies intended to understand the oceanic processes. To provide ocean analysis products on an operational basis, a new version of Global Ocean Data Assimilation System (GODAS) was configured at Indian National Centre for Ocean Information Services (INCOIS; here after INCOIS-GODAS; see section 2.1 for more detailed information about INCOIS-GODAS). Currently, various agencies in India (e.g., Indian Institute of Tropical Meteorology (IITM); Indian Meteorological Department (IMD)) are utilizing the INCOIS-GODAS ocean analysis products to initialize their coupled ocean-atmospheric models. Hence, it is important to

Responsible Editor: Aida Alvera-Azcárate

✉ Sanikommu Sivareddy
ssiva@incois.gov.in

¹ ESSO-Indian National Centre for Ocean Information Services, Hyderabad 500 090, India

² Department of Meteorology and Oceanography, Andhra University, Visakhapatnam, India

ensure that the INCOIS-GODAS produces best-quality ocean analysis. Ravichandran et al. (2013) have examined the sensitivity of INCOIS-GODAS to wind forcing using National Centers for Environmental Prediction Reanalysis-2 (NCEP-R2; Kanamitsu et al. 2002) and daily data of 3-day moving average QuikSCAT winds (here after QSCAT; Wentz et al. 2001). They have shown considerable improvement in the simulation of ocean currents over the equatorial Indian Ocean (EIO), when they replaced the model-based NCEP-R2 winds with satellite-based QSCAT winds. However, QSCAT wind data are not available since November 19, 2009. Hence, it is important to identify a suitable replacement for QSCAT wind forcing for the INCOIS-GODAS.

There are various gridded wind products available at present. These wind products are generated from atmospheric model (reanalysis products) or using the satellite data. Although the model-based products are available for research as well as operational purposes, the quality of these products are still questionable in the tropical regions compared to satellite-based products (Collins et al. 2012). For example, Uppala et al. (2005) have shown that European Centre for Medium Range Weather Forecasts Reanalysis-40 (ERA-40) winds have strong bias because of excessive precipitation and too strong Brewer-Dobson circulation in the tropical oceans. Similarly, the study by Goswami and Sengupta (2003) have shown that National Centers for Environmental Prediction-National Centre for Atmospheric Research (NCEP-NCAR) model produces erroneous precipitation patterns due to inaccurate representation of the atmospheric convective heating over the eastern tropical Indian Ocean. As suggested by Goswami and Sengupta (2003), misrepresentation of precipitation patterns in NCEP-NCAR model can produce errors in the wind fields. Hence, in general, wind products based on satellite observations are preferable than re-analysis-based wind products to use them for momentum forcing in ocean model.

After the termination of QuikSCAT, scatterometer winds are available from two satellites (1) Oceansat-2 of Indian Space Research Organisation (ISRO) and (2) Exploitation of Meteorological Satellites (EUMETSAT) Meteorological Operation-A (MetOp-A) satellites. Scatterometer winds from the former satellite, i.e., Oceansat-2, were available only for a brief period of September 23, 2009, to February 20, 2014. Hence, wind products based on Oceansat-2 scatterometer do not meet the interests of operational centers such as INCOIS who need data on near real time to provide ocean services. Scatterometer winds from EUMETSAT-MetOp-A satellites are expected to be available up to 2022. Thus, wind products based on EUMETSAT-MetOp-A can meet the requirements of operational centers. EUMETSAT MetOp-A carries Advanced Scatterometer (ASCAT; details are provided in section 2.2). Bentamy and Fillon (2012) have developed a methodology to construct a daily averaged global gridded wind

field (called DASCAT) using ASCAT and European Centre for Medium Range Weather Forecasts (ECMWF) winds. The DASCAT data are being provided by the French Research Institute for Exploration of the Sea (IFREMER), France, on operational basis with a ~2-day delay. To the best of our knowledge, this is the only operational ASCAT scatterometer level-4 wind product available online without spatial gaps. The wind product without spatial gap is an essential aspect for forcing ocean models. Precisely, this is the reason for not considering ASCAT level-3 daily products in the present study. For example, MyOcean provides ASCAT level-3 daily wind product (<http://marine.copernicus.eu/web/69-my-ocean-interactive-catalogue.php>) on operational basis. This is a pure satellite swath data without blending any numerical weather prediction model output. This ASCAT level-3 product has significant spatial gaps which make it difficult to utilize the product directly for forcing in ocean models. Sivareddy et al. (2013) have examined the quality of DASCAT winds in the tropical Indian Ocean (TIO) with respect to QSCAT winds and in situ winds from Research Moored Array for African-Asian-Australian Monsoon Analysis and Prediction (RAMA). They found that the performance of DASCAT is on par with the QSCAT. It is worth noting here that the assessments in both the studies (Bentamy and Fillon 2012; Sivareddy et al. 2013) are based on direct wind comparisons. Hence, a key question remains: whether DASCAT forcing for INCOIS-GODAS offers similar improvements in the quality of ocean analysis as the QSCAT forcing did in Ravichandran et al. (2013). Prior demonstration of the suitability of a wind product using a state-of-the-art ocean model is important before implementing it in the operational system since quality of wind have a major impact on the quality of simulated ocean currents (Sengupta et al. 2007). In the present study, we examined the suitability of the DASCAT with respect to QSCAT and NCEP-R2. Major factors that motivated the present study are (1) comparatively better performance of INCOIS-GODAS with QSCAT wind product than model-based NCEP-R2 wind product as shown by Ravichandran et al. (2013), (2) non-availability of QSCAT wind vectors after November, 2009, and also (3) ASCAT measurements which are expected to continue up to 2022. We presume that the information acquired through the analysis of the present study will be useful for those who use operational products of INCOIS-GODAS.

The present study is based on the analysis during the period from April 1, 2009, to October 31, 2009, due to (1) the common data available between QSCAT and DASCAT (for the generation of DASCAT, 12.5-km resolution ASCAT level-2b wind is used only from March 3, 2009, whereas 25-km resolution ASCAT level-2b wind was used prior to this date) and (2) the amount of model time needed to adjust to new wind forcing (DASCAT) especially for the upper ocean. The DASCAT experiment was started from May 1, 2007, and the

initial condition for this experiment was taken from QSCAT wind-based experiment. Further details on the selection of initial conditions are given in the next section. Although INCOIS-GODAS offers a global ocean analysis, we restricted our analysis for the EIO only. This is due to the fact that earlier studies in the Indian Ocean have shown that momentum flux has a significant impact on simulated ocean currents (Sengupta et al. 2007; Agarwal et al. 2008). Ravichandran et al. (2013) have also shown significant differences in the simulated ocean currents especially in the EIO, when INCOIS-GODAS is forced with different momentum fluxes. Moreover, the differences in other ocean fields (temperature, salinity, and sea surface height) are in general not significant. Similar results are found in the present study also, which can be attributed to the assimilation of temperature and salinity data into the INCOIS-GODAS. These results motivated us to focus on the improvement of ocean current simulation in the EIO using different momentum fluxes. Limiting our analysis to EIO is also due to the excellent availability of RAMA surface current data (relatively more moorings in the EIO compared to other regions of the tropical Indian Ocean) for validation during the study period.

The paper is organized as follows. Section 2 describes data sets, model, and experiments performed. The impact of different momentum fluxes on simulated ocean currents and plausible mechanism for observed differences are examined in section 3. The summary is reported in section 4.

2 Description of the model, experiments, and data set used for validation

2.1 Description about the assimilation system and model spin-up

The assimilation system used for the present study is INCOIS-GODAS, which is an ocean general circulation model (OGCM) with 3D-VAR assimilation scheme (Behringer and Xue 2004, and Ravichandran et al. 2013). The OGCM is Z-coordinate-based Modular Ocean Model (MOM) 4.0. The model has uniform zonal resolution of 0.5° and a variable meridional resolution of 0.25° within 10° of the equator, which decreases exponentially from 10° N (10° S) to 30° N (30° S) to maintain a 0.5° meridional resolution pole-wards from 30° N (30° S). There are 40 vertical layers, with 10-m resolution between surface to 240-m depth. Model integration time step is 30 min. Vertical mixing follows the non-local K-profile parameterization of Large et al. (1994). The horizontal mixing of tracers uses the iso-neutral method developed by Gent and McWilliams (1990). The Smagorinsky viscosity scheme, with Smagorinsky isotropic viscosity coefficient set to 0.9, is used for the horizontal momentum viscosity. Bryan-Lewis diffusivity model (Bryan and

Lewis 1979) is used to account for background horizontal/vertical diffusivities. The horizontal diffusivities are roughly $0.3 \times 10^{-4} \text{ m}^2 \text{ s}^{-1}$ ($1.3 \times 10^{-4} \text{ m}^2 \text{ s}^{-1}$) in the upper (deep) ocean and are time dependent.

The 3D-VAR assimilation scheme implemented in INCOIS-GODAS assimilates observed in situ temperature and salinity profiles within 60° S– 60° N and from the surface to a 750-m depth. The assimilation is performed once in 6 h. For the assimilation, observations from various platforms (Argo, eXpendable BathyThermographs (XBTs), Conductivity-Temperature-Depth (CTD), eXpendable CTD, moored buoys) during -10 days to $+10$ days of the assimilation cycle are used. Before performing the assimilation, the model is stabilized by spinning it up using climatological forcing until it reaches the equilibrium and then by performing interannual run using interannual forcing. In the next step, the model is trained with observed in situ temperature and synthetic salinity (generated by using observed in situ temperature profile and local climatological temperature and salinity relation) profiles for ~ 10 years (here after standard GODAS run). After these exercises, the assimilation system was allowed to take observed in situ temperature and salinity profiles. Observed in situ temperature and salinity profiles are assimilated in INCOIS-GODAS from 2003 onwards. By default, the assimilation system uses NCEP-R2 (Kanamitsu et al. 2002) radiation, freshwater, and momentum fluxes as atmospheric forcing. The ocean analysis obtained from the INCOIS-GODAS is found to be reasonably accurate. More details about the assimilation system and the quality of the ocean analysis can be obtained from Ravichandran et al. (2013).

2.2 Description of satellite-based and reanalyzed gridded wind products

As indicated in the introductory section, the present study employs three-gridded wind products (1) NCEP-R2—daily averaged gridded winds from the NCEP-R2, (2) QSCAT—satellite-based daily gridded winds from 3-day moving averages of scatterometer winds onboard QuikSCAT, and (3) DASCAT—satellite-based daily gridded winds from ASCAT and ECMWF merged winds. The NCEP-R2 winds (Kanamitsu et al. 2002) are obtained from a state-of-the-art atmosphere-ocean coupled analysis and forecast system, which assimilate data from 1979 through the recent years. The system uses the T62/28-level National Centers for Environmental Prediction (NCEP) global spectral model for atmosphere and MOM-3 for ocean (Kanamitsu et al. 2002; Kalnay et al. 1996). Atmospheric observations that are assimilated into the global spectral model include rawinsonde, surface marine data, aircraft data, surface land synoptic data, satellite sounder data, and surface and cloud drift winds from

satellites. NCEP-R2 winds are available at ~210-km spatial resolution.

The QuikSCAT products of ocean surface winds at a 10-m height are based on observations from SeaWinds scatterometer onboard the QuikSCAT satellite launched by National Aeronautics and Space Administration (NASA)/Jet Propulsion Laboratory (JPL). The SeaWinds uses rotating dish antenna with two spot beams that sweep in a circular pattern. The antenna radiates microwave pulses at a frequency of 13.4 GHz (Ku band) across broad regions on earth's surface. The instrument collects data with a 1800-km-wide swath during each orbit and provides ~90 % coverage of earth's ocean every day. Utilizing SeaWinds observations, a spatially complete daily gridded wind product (level 3) is generated and distributed through www.remss.com after applying a 3-day running average to fill the data gaps available in daily swaths. This product (referred as QSCAT in the present study) is available at 0.25° spatial resolution. The QSCAT wind products are not available now due to termination of QuikSCAT mission in November, 2009.

The EUMETSAT/METOP-A satellite launched on October 19, 2006, accommodated the ASCAT for measuring winds. ASCAT operates at the 5.3-GHz frequency band (C band). In general, the performance of C band in estimating wind during rain is better compared to Ku band (Lin et al. 2015). ASCAT uses fan-beam geometry with antennas oriented at an angle of 45°, 90°, and 135° with respect to satellite track. It covers two 550-km swaths which are separated from the satellite ground track by about 336 km for the minimum orbit height. Compared to QuikSCAT, ASCAT has a narrower swath. ASCAT-fixed viewing geometry generally leads to higher quality and/or higher resolution wind vectors than QuikSCAT varying geometry, which is sub-optimal in the nadir region of the swath (Vogelzang et al. 2011). As mentioned in the introductory section, a daily gridded 0.25° spatial resolution ASCAT level-4 gridded wind product (referred as DASCAT) using ASCAT level-2b winds and ECMWF wind analyses was generated based on the krigging method by Bentamy and Fillon (2012). The ECMWF wind fields are considered as external drift for the krigging method.

Comparison between the performances of QSCAT and DASCAT (based on ASCAT level-2b with spatial resolution of 12.5 km) with respect to in situ wind measurements from RAMA buoys has been carried out in the TIO by Sivareddy et al. (2013). They have shown that in general, QSCAT and DASCAT are in good agreement except during rain and low wind events. Root mean square difference (RMSD) in zonal and meridional components of wind from DASCAT (QSCAT) with respect to in situ measurements of wind from RAMA are shown to be 1.08 and 1.12 m s⁻¹ (1.44 and 1.42 m s⁻¹), respectively, during no-rain conditions. During rainy days, the RMSD was found to be slightly large (e.g., RMSD of 1.44 and

2.78 m s⁻¹ for DASCAT and QSCAT, respectively, in zonal component of wind).

2.3 Experiments conducted for the present study

In the present study, we have used the global INCOIS-GODAS setup as in Ravichandran et al. (2013), except that the observed in situ salinity replaces synthetic salinity in assimilation. The use of observed salinity profiles in place of synthetic salinity improves the salinity as well as currents, especially in the equatorial regions (figure not shown) corroborating the results of Huang et al. (2008). Using this modified INCOIS-GODAS setup, we have designed various sensitivity experiments as summarized in Table 1. As mentioned in Table 1, both experiments NTS (NCEP-R2 forcing) and QTS (QSCAT forcing) were run from January 1, 2003, to October 31, 2009, using the initial condition from standard GODAS run. Experiment DTS (DASCAT forcing) was run from May 1, 2007, to October 31, 2009, because the availability of DASCAT winds is relatively consistent from this date onwards. Ocean analysis on May 1, 2007, obtained from QTS was used as the initial condition for this DTS experiments. Selection of the common initial condition from QSCAT-forced experiment instead of NCEP-R2-forced experiment is due to the better representation of oceanic features with the QSCAT wind forcing than with the NCEP-R2 wind forcing as shown by Ravichandran et al. (2013).

Evaluation of model performance is carried out using daily averaged outputs from April 1, 2009, to October 31, 2009, discarding the outputs of May 1, 2007, to March 31, 2009. This analysis period is chosen to provide sufficient time for the model to get adjusted to the new forcing. Also, it is due to the fact that before March, 2009, DASCAT winds were generated using 25-km resolution of ASCAT level-2b data, after that DASCAT winds were generated using 12.5-km resolution. It is presumed that the quality of the DASCAT product might differ with these changes. Further, DASCAT based on a 12.5-km product is continuously available as of now with a ~2-day delay, and the same is used in this study. Hence, it is appropriate to evaluate model performance during the aforementioned April 1, 2009, to October 31, 2009, period.

2.4 Data and methodology used for the evaluations

We have used both in situ and satellite-based current observations for comparing the model simulations. For in situ data, daily averaged ocean currents available from RAMA moorings (McPhaden et al. 2009) at a 10-m depth are used. We have selected data from all the RAMA locations where at least 30 days of data were available in the EIO during the analysis period of April 1, 2009, to October 31, 2009. Based on this condition, we are left with only six RAMA locations in the EIO. For spatial validation of surface currents, we have used a

Table 1 Summary of the experiments conducted using INCOIS-GODAS

Experiment	Momentum flux	Model run	Initial condition
NTS	NCEP-R2	January 1, 2003, to October 31, 2009	Standard GODAS run
QTS	QSCAT	January 1, 2003, to October 31, 2009	Standard GODAS run
DTS	DASCAT	May 1, 2007, to October 31, 2009	NTS experiment

new version of Ocean Surface Current Analysis-Real time (OSCAR) current data, prepared by Bonjean and Lagerloef (2002). The new OSCAR currents are available on $1/3^\circ$ spatial and 5-day temporal resolution. Using quasi-steady geostrophic, local wind-driven, and thermal wind dynamics, the OSCAR data processing system calculates sea surface currents from satellite altimetry, from vector wind fields, as well as from sea surface temperature (Dohan and Maximenko 2010). The technique is tuned to obtain best representation of ageostrophic motion of the 15-m drogued drifters relative to the surface wind stress. Near the equatorial regions, the new OSCAR data processing system uses a realistic shear model for the Ekman component based on Stommel (1960). This produces much more accurate results on the equator compared to an older version of OSCAR product. Also, this new version uses a unique set of orthogonal polynomial basis functions, symmetric on the equator to solve the geostrophic and Ekman terms across the equatorial singularity.

The new OSCAR provides reasonably accurate ocean surface currents off equatorial regions (Bonjean and Lagerloef 2002). Validation and error analysis of the new version of OSCAR surface currents in the Pacific Ocean carried out by Johnson et al. (2007) have shown that the OSCAR product provides reasonably accurate zonal surface current variability in the near-equatorial regions too. Moreover, Sikhakolli et al. (2013) has done a comprehensive evaluation of the OSCAR currents in the TIO. They have shown that the spatial patterns, including in the equatorial region, are well captured by OSCAR currents. They have found correlations of the order 0.75 in the equatorial region for zonal current (zonal current is dominant over meridional current in the EIO). Further, in order to examine the quality of OSCAR surface current in the EIO, we have performed a detailed validation of OSCAR surface current in the EIO using RAMA currents (Fig. 1). It can be inferred from Fig. 1 that zonal currents of OSCAR compare well with the RAMA in the EIO. Mean bias is less than 15 cm s^{-1} , RMSD is less than standard deviation (STD), and correlation is greater than 0.7. These results are consistent with the results of Sikhakolli et al. (2013) and indicate that OSCAR current data can be used as a reference for spatial validation of model-derived surface current. This new OSCAR product has been used for the model validation and to address various research problems in the TIO (Ravichandran et al. 2013; Chakraborty et al. 2014; Joseph et al.

2012). It is worth mentioning here that OSCAR depends on QuikSCAT during our analysis period and thus the validation may favor QTS with respect to DTS and NTS. Precisely, this is the reason why we have not used OSCAR data extensively except for spatial comparisons. The independent validation we provide is limited to the six RAMA buoy time series in the EIO. In the present study, we use these limited sources of in situ data and explained plausible physical mechanisms responsible for the difference in the current simulation between different wind forcing experiments. Hence, a caution should be maintained when extending results from the present study to other oceans (e.g., Pacific and Atlantic Ocean).

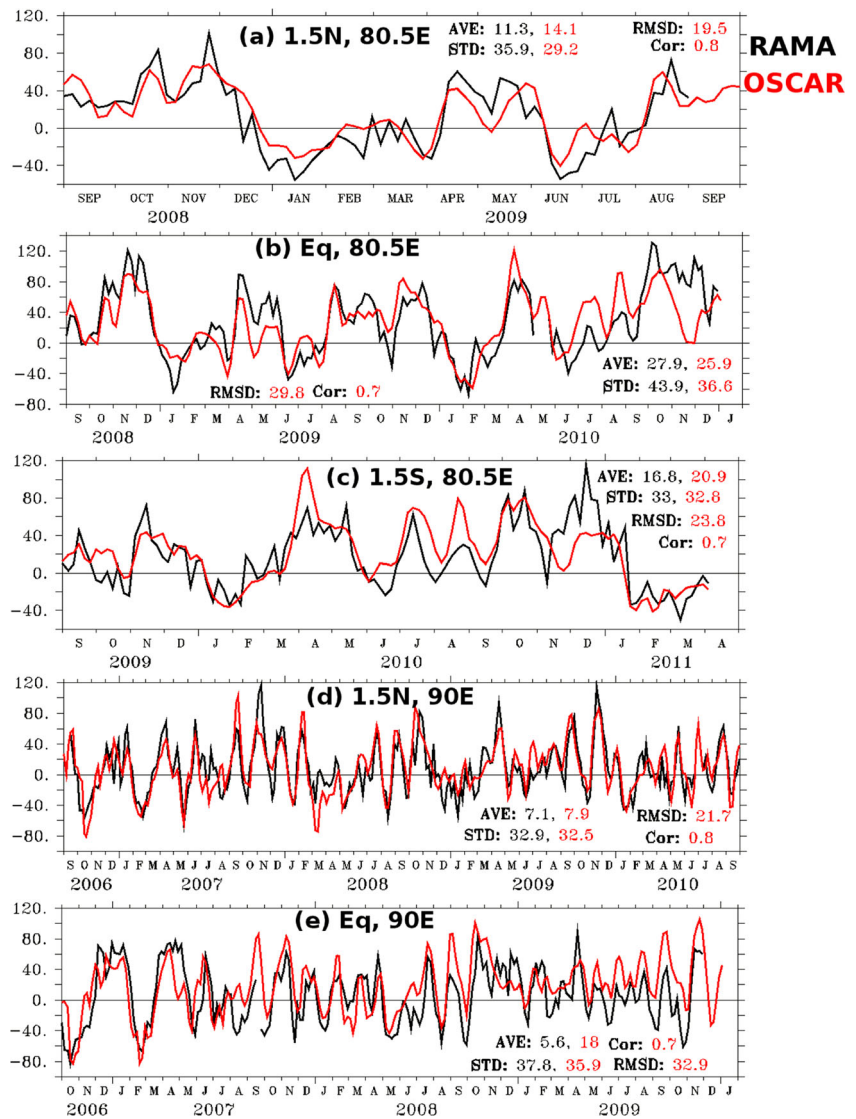
3 Results and discussion

3.1 Validation of INCOIS-GODAS simulated currents for NTS, DTS, and QTS experiments

Seasonal averages of ocean surface currents in EIO, averaged for pre-monsoon (April–May), summer monsoon (June–August), and post-monsoon (September–October), are shown in Fig. 2. It is worth mentioning here that the differences in surface currents between QTS, DTS, and NTS are not so significant in the TIO except in the EIO (figure not shown). Hence, we show comparisons between OSCAR and model simulated currents only in the EIO. From the figure, it is quite clear that both NTS and DTS show large differences in the central parts of the EIO, especially during monsoon and post-monsoon seasons. During the summer monsoon and post-monsoon seasons, OSCAR shows eastward current, whereas NTS and DTS show strong westward current in the central part of the EIO. Also, QTS surface currents show reasonable agreement with OSCAR, whereas NTS and DTS show westward bias, particularly in the central part of EIO.

In order to gain further insights, we have compared zonal (Fig. 3) and meridional (Fig. 4) current from NTS, QTS, and DTS with in situ currents from available RAMA buoys in the EIO. Comparison of simulated zonal (meridional) currents with daily averaged 10-m zonal (meridional) current observations from different RAMA mooring locations is shown in Fig. 3a–f. In the eastern part of the EIO (Fig. 3e, f), the observed zonal currents are weak (within 20 cm s^{-1}), except for few events during

Fig. 1 Comparison of zonal currents (cm s^{-1}) from daily RAMA (black) and OSCAR (red) in the EIO (a 1.5° N , 80.5° E ; b the equator, 80.5° E ; c 1.5° S , 80.5° E ; d 1.5° N , 90° E ; and e the equator, 90° E). Mean (AVE), standard deviation (STD), root mean square difference (RMSD), and correlation are also shown in the corresponding panel. For better readability of figures, 5-day smoothing is applied



pre-monsoon and post-monsoon months. Simulated zonal currents from DTS and QTS are reasonably accurate in the eastern EIO location of 1.5° N , 90° E (Fig. 3e). At the 90° E equator location, simulated zonal currents from QTS are much stronger than the observations during pre-monsoon and post-monsoon season (Fig. 3f). Except from these localized differences, both QTS and DTS current simulations appear to be fairly well in the eastern part of the EIO. In the central EIO (Fig. 3a–d), QTS follows the RAMA observation very closely whereas NTS and DTS have the westward bias, with NTS having large bias compared to DTS. For example, at equator 80.5° E during July–October, 2009, QTS and RAMA showed eastward current whereas DTS and NTS showed strong westward zonal current (Fig. 3b). Performance of QTS is better than that of the other two experiments of NTS and DTS in the southwestern parts of the EIO (figure not shown) too. Further, from the statistics summarized in Table 2, it is

clear that the mean and variability of zonal currents are very well simulated by QTS than NTS and DTS. For instance, while the maximum observed mean bias with respect to RAMA in zonal current reaches 60 cm s^{-1} in DTS and NTS, it is less than 30 cm s^{-1} for QTS.

Comparisons of meridional component of surface current from NTS, DTS, and QTS with RAMA indicate that the differences between model experiments are much smaller than the differences encountered for the zonal component comparisons. This is expected as the contribution from zonal component of currents is dominant over that from the meridional components of currents at the equator. For example, the STD of meridional component of surface currents from RAMA data is observed to be ranging from 4 to 18 cm s^{-1} in the EIO locations, while for the zonal component, it is observed to be ranging from 15 to 35 cm s^{-1} . There are only few occasions where the magnitude of meridional component of current exceeds 20 cm s^{-1} whereas the magnitude of zonal

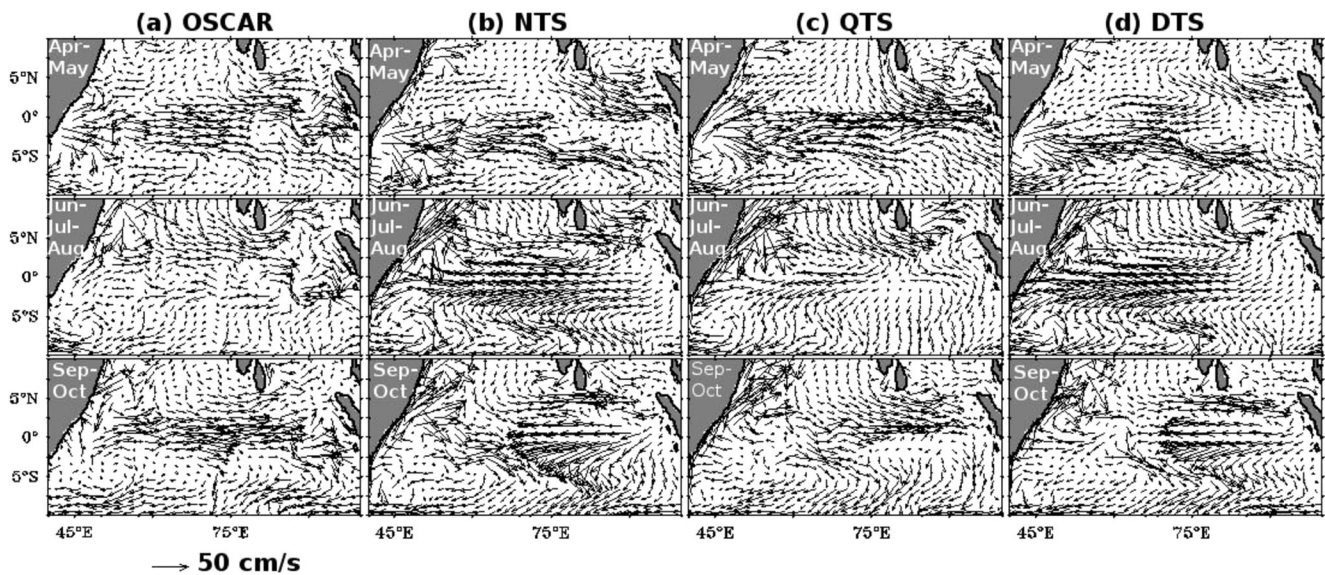


Fig. 2 Seasonally averaged (April–May (*top panel*), June–August (*middle panel*), and September–October (*bottom panel*)) ocean surface currents (cm s^{-1}) from **a** OSCAR and simulated currents averaged over the upper 30 m (cm s^{-1}) from **b** NTS, **c** QTS, and **d** DTS during the year 2009

component of current is more than 20 cm s^{-1} during most of the study period. It is important to note that, in general, simulated meridional component of surface current from three different model experiments match well with the observations (Fig. 4). For example, low-magnitude cross-equatorial current observed from RAMA in the central (Fig. 4a, b) and eastern parts (Fig. 4e, f) is captured by model experiments with a reasonable skill. Satellite-based wind forcing experiments QTS and DTS show slightly better current simulations than NTS, which is clearly evident from the correlation listed in Table 2.

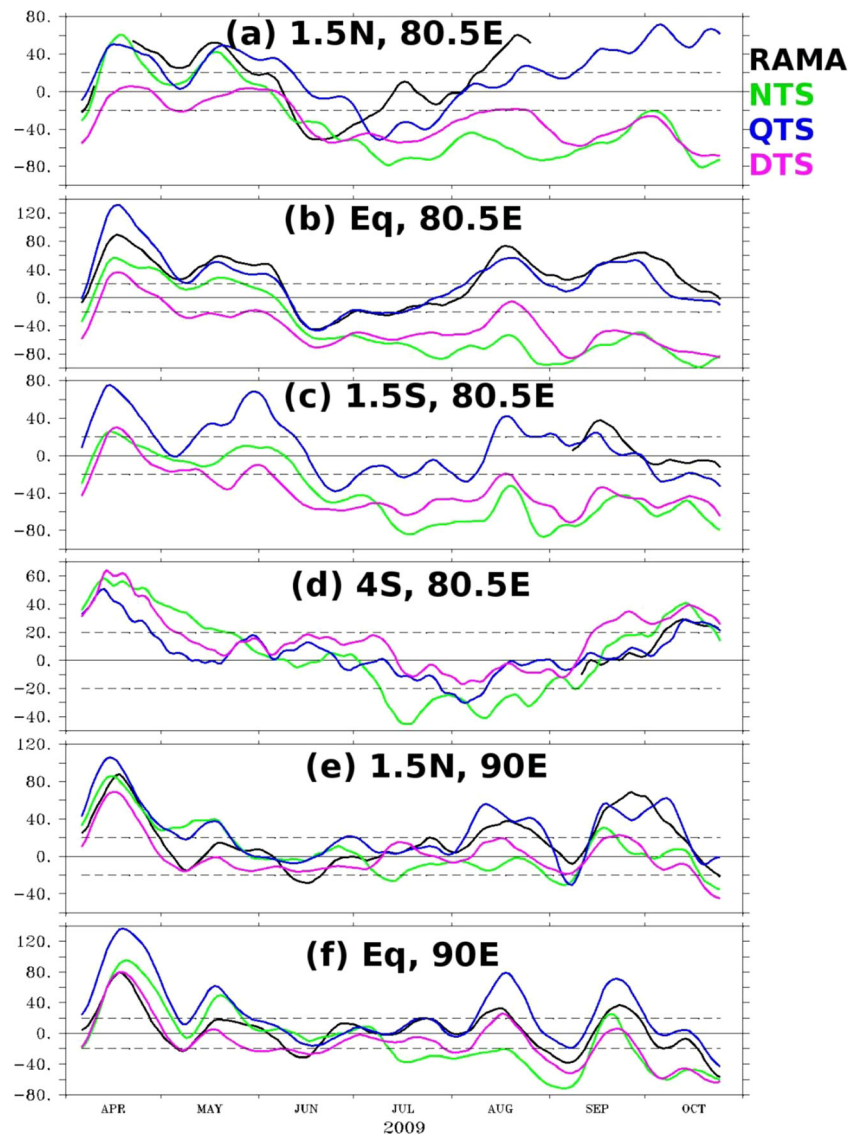
From the above, it is clear that the results from the comparisons of model simulated currents with OSCAR (Fig. 2) and in situ RAMA currents are consistent with each other. The results of QTS and NTS are consistent with the results of Ravichandran et al. (2013) as well. From the above analysis, it is also clear that DASCAT- and QSCAT-derived surface currents are better than NCEP-R2-derived surface currents. Less accurate representation of currents by NCEP-R2 wind-forced experiment, compared to other two wind-forced experiments, is understandable, since the quality of NCEP-R2 winds is low in the eastern parts of the TIO as discussed by Goswami and Sengupta (2003). Such errors are relatively less in the satellite-blended wind products and thus offer better simulation of ocean currents in the ocean model as shown by Sengupta et al. (2007). Since the causes and impacts of discrepancies between NCEP-R2 and QSCAT in ocean models are already examined in detail in the earlier studies (Sengupta et al. 2007; Agarwal et al. 2008; Ravichandran et al. 2013), we are not going to elaborate on this further. On the other hand, relatively less accurate representation of currents in DTS compared to QTS in the equatorial region indicates that there must be significant discrepancies between the

DASCAT and QSCAT wind products. The probable reason for these discrepancies in the wind products is examined in the following section. Since the differences between performances of model experiments are more pronounced at the equator and in the zonal component of currents, the remaining part of the discussions is focused on zonal components only.

3.2 Why DASCAT-forced currents are not better than QSCAT-forced currents?

Figure 5a, b shows zonal wind patterns along the equator from QSCAT and DASCAT during the analysis period. Occurrence of westerly wind events in intra-seasonal time scale is clearly noticeable in Fig. 5. As suggested by Goswami and Sengupta (2003), the westerly wind events observed throughout the year are responses to the intra-seasonal variations of convective activity. Earlier studies have shown that these wind events generate intra-seasonal current variability in the EIO (Senan et al. 2003). It is clear from Fig. 5 that the magnitude and spatiotemporal extent of these westerly wind events are relatively weak in DASCAT than in QSCAT. As mentioned earlier, DASCAT winds are constructed using satellite-based ASCAT winds and model-based ECMWF winds (Bentamy and Fillon 2012). As reported by Bentamy and Fillon (2012), ASCAT and collocated DASCAT poorly correlates (correlation of 0.85) at the equator than at other regions, due to less coverage of ASCAT retrievals and low quality of ECMWF winds at the equator. Their study also showed that the high wind events ($>12 \text{ m s}^{-1}$) observed from the ASCAT measurements are smoothed by the objective method used to construct DASCAT. This smoothness has resulted in the underestimation of magnitude of

Fig. 3 Ocean surface zonal currents from RAMA moorings (black), NTS (green), QTS (blue), and DTS (pink) at **a** 1.5° N, 80.5° E; **b** Eq, 80.5° E; **c** 1.5° S, 80.5° E; **d** 4° S, 80.5° E; **e** 1.5° N, 90° E; and **f** Eq, 90° E. The model currents are interpolated to RAMA buoy location and averaged in upper 30 m. For better readability of figures, all the time series have been smoothed with a 5-day running mean. Statistics for model simulated daily zonal surface currents are computed with respect to the daily zonal surface current data from RAMA observations. Units are in centimeters per second



wind in DASCAT in the high wind condition. They have also indicated that discrepancies are large at small scales in terms of wind amplitude. Sivareddy et al. (2013) have shown underestimation of zonal wind variability in DASCAT (STD, 4.88 m s^{-1} for no-rain and 7.74 m s^{-1} for high wind) compared to QSCAT (STD, 5.3 m s^{-1} for no-rain and 8.03 m s^{-1} for high wind) and RAMA (STD, 5.2 m s^{-1} for no-rain and 8.44 m s^{-1} for high wind) during both rain-free and high wind events.

It can be hypothesized from the above discussion that the degradation in the quality of wind at the equator in DASCAT compared to QSCAT is the source for the observed discrepancies between the zonal currents of QTS and DTS in the central parts of the EIO. However, it is not clear why major discrepancies in the simulated current fields of DTS and QTS are observed only in the central parts of the EIO. Hence, in order to further understand the

differences between DTS and QTS current simulations in the central parts of the EIO, we have examined zonal momentum budget in the central EIO.

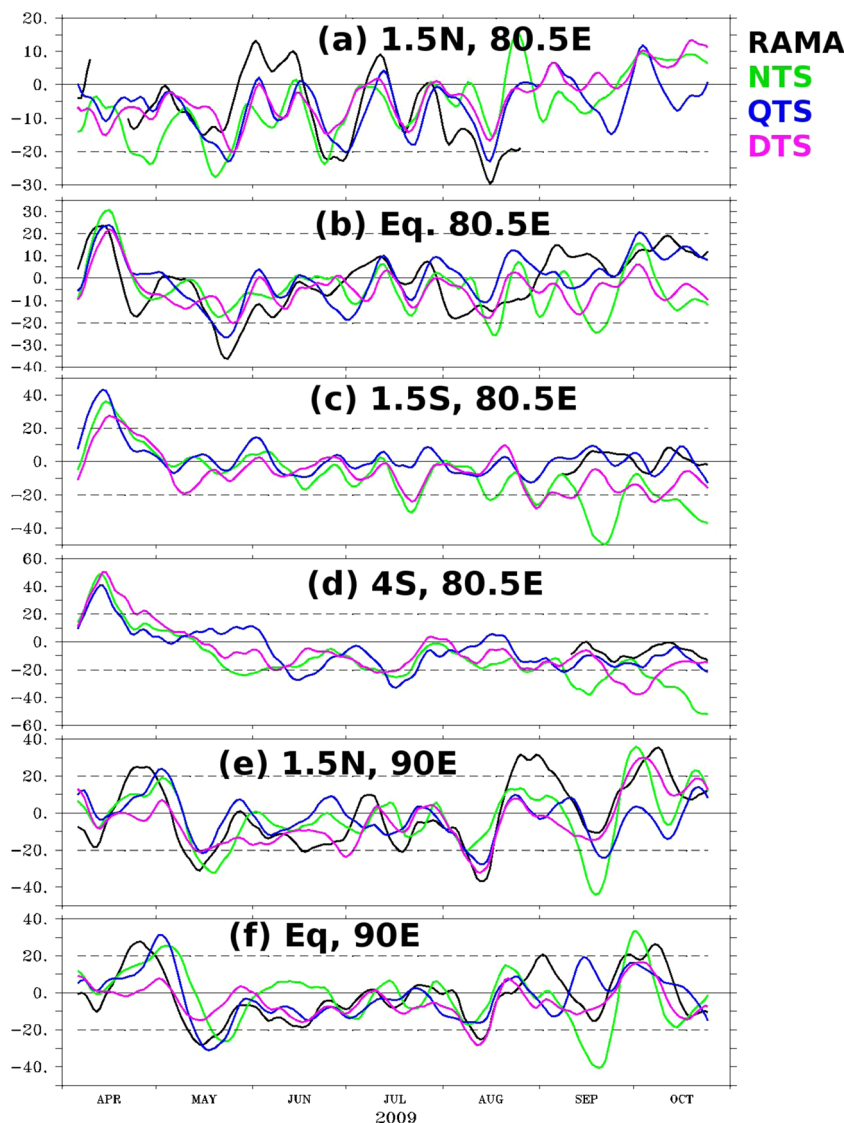
3.3 Zonal momentum budget for the central equatorial Indian Ocean

According to Sengupta et al. (2007), zonal momentum budget can be represented as

$$\frac{\partial u}{\partial t} = -\frac{1}{\rho} \frac{\partial p}{\partial x} + \frac{\partial}{\partial z} \left(k \frac{\partial u}{\partial z} \right) + \text{other term}$$

where u , ρ , p , and k are zonal current speed (m s^{-1}), density of sea water (kg m^{-3}), pressure (N m^{-2}), and coefficient of the vertical momentum mixing ($\text{m}^2 \text{ s}^{-1}$), respectively; independent variables t , x , and z represent time (s), longitude (m),

Fig. 4 Same as Fig. 3 except for meridional component of current



and depth (m), respectively. The first term on the right-hand side is known as the zonal pressure gradient (ZPG) term. This is obtained using model dynamic height in the upper 120-m ocean layer. The second term is the zonal wind stress (ZWS) term; integration of the stress from a sufficiently deep level (~120 m) to the surface gives the model surface boundary condition: $k(z=0) \frac{\partial u}{\partial z} |_{z=0} = \tau_x$, where τ_x is zonal wind stress per unit mass per unit depth ($m^2 s^{-2}$). The “other terms” includes zonal, vertical, and meridional advection. These are not considered in the present study as the zonal momentum balance at the equator is dominated by the ZPG and ZWS (Sengupta et al. 2007).

Earlier studies (e.g., Bubnov 1994, Sengupta et al. 2007, and others) have shown that zonal currents in the upper 120 m in the EIO, especially eastern parts (east of 60° E, where large differences between QTS and DTS were observed), are influenced mainly by ZWS and ZPG terms. The ZPG is westward throughout the year, except in February and March (Bubnov

1994 and Sengupta et al. 2007). On intra-seasonal time scales, the ZPG is largely influenced by ZWS (e.g., westerly wind bursts) via equatorial waves (Sengupta et al. 2007). In order to understand the relative contribution of ZPG and ZWS on zonal current acceleration in the central EIO (2° S–2° N and 60° E–90° E; CEIO), we have examined the depth-wise correlation between ZWS and zonal current acceleration and between ZWS+ZPG and zonal current acceleration (Fig. 6). The correlation between ZWS and zonal current acceleration is between 0.6 and 0.7 in the upper 60-m layer. It indicates that around 36–49 % of zonal acceleration can be explained by ZWS term alone. When ZPG term is added to the ZWS term, the correlation increased to 0.8–0.9 in the upper 60-m layer. This indicates that about 70–80 % of zonal current variation in the CEIO can be explained by these two terms. This result is consistent with the results of Sengupta et al. (2007). It can be inferred from these results that the contribution from ZPG to total acceleration term is 28–32 % and is comparable to that of

Table 2 Summary from the statistical comparison of surface zonal and meridional currents at various RAMA locations in the equatorial Indian Ocean (EIO)

Location	No. of points	Mean (cm s ⁻¹)		Bias (cm s ⁻¹) with respect to RAMA (Model-RAMA)			Standard deviation (cm s ⁻¹)			Root mean square difference (cm s ⁻¹) w.r.t RAMA			Correlation model vs RAMA		
		RAMA	NTS	QTS	DTS	RAMA	NTS	QTS	DTS	RAMA	NTS	QTS	DTS	NTS	QTS
1.5° N and 80.5° E	132	U 8.9	-36.1	-3.6	-34.9	32.7	38.1	28.2	20.2	51.2	27.3	41.5	0.5	0.6	0.7
		V -7.7	-1.9	-0.9	0.7	10.5	8.8	7.1	5	12.6	8.9	9.7	0.2	0.6	0.4
Eq and 80.5° E	203	U 2.6	-66.4	-2	-67.7	34.8	46.8	38.4	28.6	79.5	16.6	73.3	0.5	0.9	0.6
		V -1.4	-3	1.8	-3.5	12.8	10.6	10.6	7.6	13.8	10.4	12.4	0.3	0.6	0.4
1.5° S and 80.5° E	48	U 5.8	-64.1	-12.4	-54.6	15.9	10.7	17.8	8.9	66.2	15.1	56.3	0.3	0.9	0.5
		V 0.6	-26.6	0.4	-15.3	4.9	12.3	5.6	5.7	30.8	6.2	16.2	-0.6	0.3	0.5
4° S and 80.5° E	45	U 11.9	7	0.4	17.3	12.3	15.2	10.2	7.1	10.5	4.9	19.5	0.9	0.9	0.7
		V -6.9	-23.7	-6.4	-13.4	4.2	10.8	4.3	9.6	26.7	6.9	15.8	-0.2	0.8	0.5
1.5° N and 90° E	203	U 17.4	-10.1	8.7	-16.5	26.8	27	28.3	21.2	27.6	17.2	22.5	0.5	0.9	0.8
		V -0.8	-1.4	-1.8	-3.8	17.8	15.2	10.7	13.1	14.5	15.9	12.7	0.6	0.5	0.7
Eq and 90° E	203	U 3.8	-12.2	22.8	-15.1	25.4	39.5	39	29.9	31.2	31.2	20.7	0.7	0.9	0.9
		V -2	0.3	0.1	-3	13.7	14.7	12.4	8.5	14.7	10.9	10.4	0.5	0.7	0.7

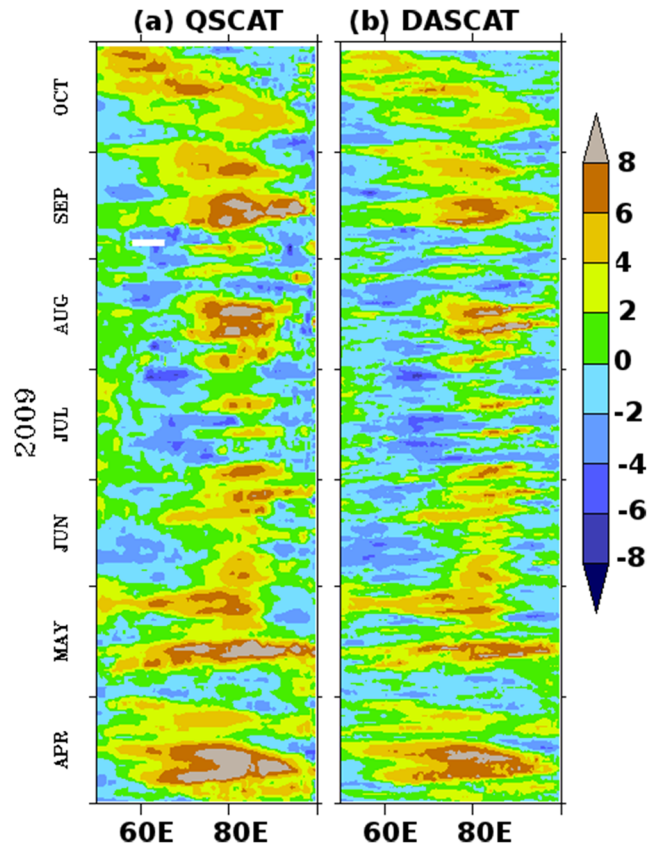


Fig. 5 Longitude-time sections of zonal wind speed (m s⁻¹) averaged for 2° S–2° N from **a** QSCAT and **b** DASCAT during the period April 1, 2009, to October 31, 2009

ZWS contribution (36–49 %). Hence, the remaining part of this section deals on the link between zonal current acceleration and other two terms, i.e., ZWS and ZPG.

ZWS and ZPG averaged over the CEIO corresponding to QTS and DTS experiments are shown in Fig. 7. The ZPG is negative (westward) throughout the analysis period corroborating the results of Bubnov (1994) and Sengupta et al. (2007). On the other hand, ZWS is positive (eastward) throughout the study period. Further, the amplitude of ZWS is large compared to ZPG. Large amplitudes of ZWS are associated with the westerly wind bursts (compare Fig. 5 with Fig. 7), which typically last for 10–40 days (Sengupta et al. 2007). It is clear from Fig. 7 that discrepancies in ZPG between QTS and DTS experiments are very small compared to discrepancies in ZWS between QTS and DTS experiments. For example, the magnitude of difference is less than $0.5 \times 10^{-7} \text{ m s}^{-2}$ (equivalent to $\sim 0.5 \text{ m s}^{-1}$ error in the surface wind) for ZPG, while it reaches $3 \times 10^{-7} \text{ m s}^{-2}$ (equivalent to $\sim 3 \text{ m s}^{-1}$ error in the surface wind) for ZWS (Fig. 8a). It is worth to remind here that the temperature and salinity profiles are assimilated using 3D-VAR in INCOIS-GODAS. This assimilation corrects the model ZPG. Hence, the insignificant differences between ZPG of QTS and DTS are due to the assimilation of temperature and salinity profiles in INCOIS-GODAS (figure not shown).

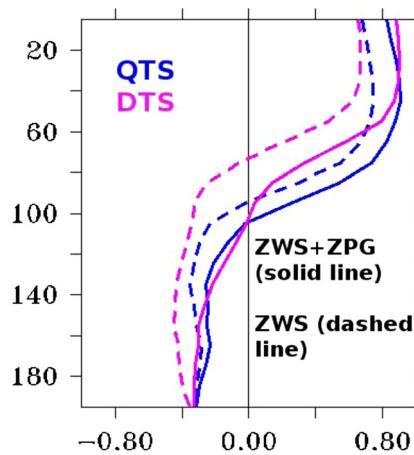
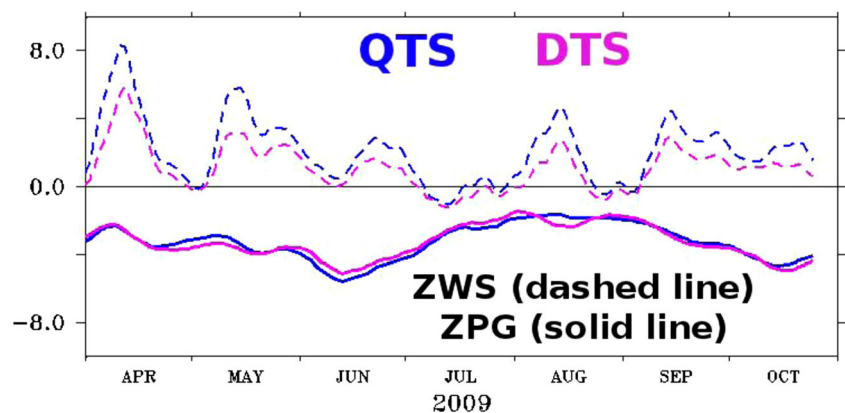


Fig. 6 Correlation between zonal current acceleration and ZWS (dashed line) and between zonal current acceleration and ZWS+ZPG (solid line). Results from the experiments corresponding to QSCAT and DASCAT forcing are shown in blue and pink colour, respectively. Zonal current acceleration, ZWS, and ZWS+ZPG terms are averaged for central equatorial Indian Ocean (2° S–2° N and 60° E–90° E; CEIO) and all the variables are smoothed by 10-day running mean before performing correlations. The correlation greater than 0.4 is significant at 95 % confidence level

Large differences in ZWS compared to ZPG between QTS and DTS are obviously due to the discrepancies in the local wind forcing (compare Fig. 5 with Fig. 7). These results indicate that the discrepancies, in the zonal current patterns in the CEIO, between QTS and DTS experiments are primarily explained by the local discrepancies (ZWS represent local effect) between DASCAT and QSCAT winds. In order to get further clarity on these results, we have analyzed the differences in budget terms between QTS and DTS experiments.

Figure 8 shows the difference between QTS and DTS in terms of difference in (a) ZPG, ZWS, and ZPG+ZWS along with (b) the difference between QTS and DTS in total zonal acceleration. As discussed earlier, differences (DTS-QTS) in ZWS are larger compared to differences in ZPG. Due to the dominance of the difference in ZWS, compared to the difference in ZPG, the difference in ZPG+ZWS shows good temporal correspondence with the difference in ZWS (Fig. 8a). Further, the difference in ZWS (and also ZWS+ZPG) is

Fig. 7 Time series of ZPG (10^{-7} m s^{-2} , solid line) and ZWS (10^{-7} m s^{-2} , dashed line) from QTS (blue) and DTS (pink) experiment. All the variables are smoothed by 10-day and averaged for the CEIO (2° S–2° N and 60° E–90° E) before performing calculations



negative throughout the study period with large differences in April, May, August, and October. Interestingly, the difference between the zonal current acceleration of DTS and QTS (DTS-QTS) is negative during these months with overall good temporal correspondence between the difference in ZWS (and also ZPG+ZWS) and difference in zonal current, extending up to 100 m deep. This confirms the impact of local wind differences on the discrepancies in zonal current (Fig. 8b) as discussed earlier.

From the above discussions, we were able to find answers to the following questions.

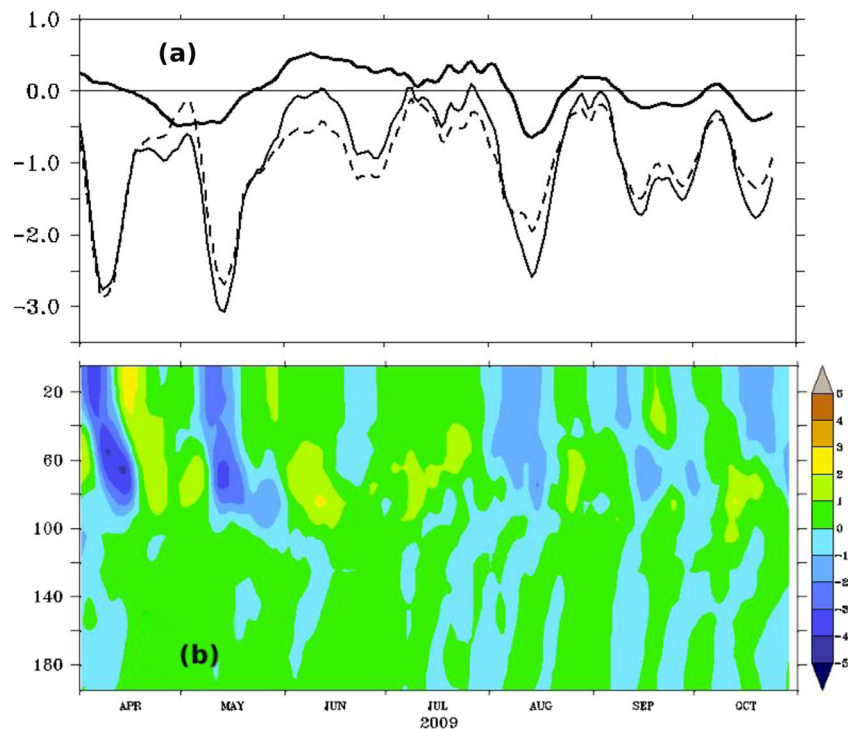
- (1) Why are the differences between QTS and DTS in the simulation of currents found only in the central part of the equatorial Indian Ocean?
- (2) Why do the model simulated currents of DTS have westward bias in the central part of the equatorial Indian Ocean?

The answer to the first question is that the contribution from the ZPG, which represents both local and remote wind effect, is very small for the difference in currents between DTS and QTS, due to the assimilation of temperature and salinity profiles in INCOIS-GODAS. The contribution from ZWS, which represents the local wind effect, is major for the differences in currents between DTS and QTS in the CEIO. The answer for the second question is that the eastward-acting ZWS is inferior to the westward-acting ZPG in the DASCAT-forced model experiment.

4 Summary and conclusion

This study examines the suitability of DASCAT momentum flux, with respect to QSCAT and NCEP-R2 momentum flux, for forcing the INCOIS-GODAS by analyzing the simulated surface currents. The motivations for the present study are (1) better accuracy of satellite-based wind products than NCEP-R2 winds, (2) non-availability

Fig. 8 Difference between DASCAT and QSCAT (DASCAT-QSCAT) wind-forced experiments in terms of differences in **a** ZWS (10^{-7} m s^{-2} , dashed line), ZPG (10^{-7} m s^{-2} , thick solid line), and ZWS+ZPG (10^{-7} m s^{-2} , thin solid line) and **b** depth-wise zonal current acceleration (10^{-7} m s^{-2}). All the variables are smoothed by a 10-day running mean and averaged for the CEIO (2° S – 2° N and 60° E – 90° E) before performing calculations



of satellite-based QuikSCAT winds after November, 2009, and (3) anticipated availability of ASCAT wind measurements up to 2022. For this purpose, we have designed three experiments by forcing INCOIS-GODAS with the three different momentum fluxes (NCEP, QSCAT, and DASCAT) and analyzed simulated upper ocean currents. Over off-equatorial regions in the TIO, the DASCAT-forced simulated surface currents are on par with QSCAT one. However, in the EIO, the QSCAT-forced simulated currents are relatively better than DASCAT-forced simulated currents. It appears that lack of small-scale variability in DASCAT, especially during high wind events, leads to less accurate simulation of upper ocean current in the EIO. Nevertheless, DASCAT-forced simulated upper ocean currents are better than NCEP-R2-forced simulated upper ocean currents. Thus, in the absence of QSCAT winds, it is better to use momentum flux derived from DASCAT instead of NCEP-R2, in INCOIS-GODAS, for providing better ocean analysis.

The present study also has provided valuable insights on the impact of errors in wind on the simulated ocean currents. It is found that the impact of the wind discrepancies between DASCAT and QSCAT is majorly local and confined to the upper 100 m of water column. The less impact of error in wind on ocean analysis of INCOIS-GODAS is largely attributed to the correction of ZPG by the assimilation of temperature and salinity profiles. Since the impact of wind discrepancies is felt in assimilation-enabled INCOIS-GODAS model, the impact is presumed to be larger in ocean forecasts. Apart from finding

a suitable wind product for the state-of-the-art ocean models like INCOIS-GODAS, the present study demonstrates the need for careful evaluation of available wind products using ocean model simulations.

Acknowledgments The encouragement and facilities provided by the Director, INCOIS, are gratefully acknowledged. We would like to thank Dr. Suprith Kumar, INCOIS, and Dr. Uday Bhaskar, INCOIS, for their valuable suggestions towards improving this manuscript. We thank IFREMER for providing DASCAT wind fields through Asia-Pacific Data-Research Center website. QuikSCAT data are produced by Remote Sensing Systems (www.ssmi.com) and sponsored by the NASA Ocean Vector Winds Science Team (www.remss.com). The model experiments are designed and ran on INCOIS-High Performance Computing (HPC) machine. We thank INCOIS-HPC team for their technical support. Graphics are generated using Ferret. We gratefully acknowledge the support provided by Earth System Science Organization, Ministry of Earth Sciences, Government of India, to conduct this research. This is INCOIS contribution No. 228.

References

- Agarwal N, Sharma R, Basu S, Sarkar A, Agarwal VK (2008) Evaluation of relative performance of QuikSCAT and NCEP re-analysis winds through simulations by an OGCM. *Deep-Sea Res I*. 54(8):1311–1328
- Behringer DW, Xue Y (2004) Evaluation of the global ocean data assimilation system at NCEP: the Pacific Ocean, paper presented at the Eighth symposium on Integrated Observing and Assimilation System for Atmosphere, Ocean, and Land Surface. Am Meteorol Soc, Seattle, Wash, 11-15

- Bentamy A, Fillon DC (2012) Gridded surface wind fields from Metop/ASCAT measurements. *Int J Remote Sens* 33(6):1729–1754
- Bonjean F, Lagerloef GSE (2002) Diagnostic model and analysis of the surface currents in the tropical Pacific Ocean. *J Phys Oceanogr* 32: 2938–2954
- Bryan K, Lewis LJ (1979) A water mass model of the world ocean. *J Geophys Res* 84:2503–2517
- Bubnov VA (1994) Climatic zonal pressure gradient in the equatorial zone of the Indian Ocean. *Oceanography* 33:414–420
- Chakraborty A, Sharma R, Kumar R, Basu S (2014) An OGCM assessment of blended OSCAT winds. *J Geophys Res* 119:173–186. doi:10.1002/2013JC009406
- Collins C, Reason CJC, Hermes JC (2012) Scatterometer and reanalysis wind products over the western tropical Indian Ocean. *J Geophys Res* 117, C03045. doi:10.1029/2011JC007531
- Dohan K, Maximenko N (2010) Monitoring ocean currents with satellite sensors. *Oceanography* 23(4):94–103. doi:10.5670/oceanog.2010.08
- Gent PR, McWilliams JC (1990) Isopycnal mixing in ocean circulation models. *J Phys Oceanogr* 20:150–155
- Goswami BN, Sengupta D (2003) A note on the deficiency of NCEP/NCAR reanalysis surface winds over the equatorial Indian Ocean. *J Geophys Res* 108(C4):3124. doi:10.1029/2002JC001497
- Huang, Boyin, Xue, Yan, Behringer D (2008) Impacts of Argo salinity in NCEP Global ocean data assimilation system: the tropical Indian Ocean. *J Geophys Res* v 113:C08002. doi:10.1029/2007JC004388
- Johnson ES, Bonjean F, Lagerloef GSE, Gunn JT (2007) Validation and error analysis of OSCAR sea surface currents. *J Atmos Ocean Technol* 24:688–701. doi:10.1175/JTECH1971.1
- Joseph S, Wallcraft AJ, Jensen TG, Ravichandran M, Shenoi SSC, Nayak S (2012) Weakening of spring Wyrki jets in the Indian Ocean during 2006–2011. *J Geophys Res* 117, C04012. doi:10.1029/2011JC007581
- Kalnay E, Kanamitsu M, Kisteler R, Collins W, Deaven D, Gandin L, Iredell M, Saha S, White G, Woolen J, Zhu Y, Chelliah M, Ebisuzaki W, Higgins W, Janowiak J, Mo KC, Ropelewski C, Wang J, Leetmaa A, Reynolds R, Jenne R, Joseph D (1996) The NCEP/NCAR 40-year reanalysis project. *Bull Am Meteorol Soc* 77(3): 437–471
- Kanamitsu M, Ebisuzaki W, Woollen J, Yang SK, Hnilo JJ, Fiorino M, Potter GL (2002) NCEP-DOE AMIP-II reanalysis (R-2). *Bull Am Meteorol Soc* 83:1631–1643
- Large WG, McWilliams JC, Doney SC (1994) Oceanic vertical mixing: a review and model with a nonlocal boundary layer parameterization. *Rev Geophys* 32:363–403
- Lin W, Portabella M, Stoffelen A, Verhoef A, Turiel A (2015) ASCAT wind quality control near rain. *IEEE Trans Geosci Rem Sens* 53(8): 4165–4177. doi:10.1109/TGRS.2015.2392372
- McPhaden MJ, Meyers G, Ando K, Masumoto Y, Murty VSN, Ravichandran M, Syamsudin F, Vialard J, Yu L, Yu W (2009) RAMA the research moored array for African–Asian–Australian monsoon analysis and prediction a new moored buoy array in the historically data-sparse Indian Ocean provides measurements to advance monsoon research and forecasting. *Bull Am Meteorol Soc* 90: 459–480. doi:10.1175/2008BAMS2608.1
- Ravichandran M, Behringer D, Sivareddy S, Girishkumar MS, Chacko N, Harikumar R (2013) Evaluation of the global ocean data assimilation system at INCOIS: the tropical Indian Ocean. *Ocean Modell* 69:123–135. doi:10.1016/j.oceanmod.2013.05.003
- Senan R, Sengupta D, Goswami BN (2003) Intraseasonal “monsoon jets” in the equatorial Indian Ocean. *Geophys Res Lett* 30:1750. doi:10.1029/2003GL017583
- Sengupta D, Senan R, Goswami BN, Vialard J (2007) Intraseasonal variability of equatorial Indian Ocean zonal currents. *J Clim* 20:3036–3055. doi:10.1175/JCLI4166.1
- Sikhakolli R, Sharma R, Basu S, Gohil BS, Sarkar A, Prasad KVS (2013) Evaluation of OSCAR ocean surface current product in the tropical Indian Ocean using in situ data. *J Earth Syst Sci* 122(1):187–199
- Sivareddy S, Ravichandran M, Girish Kumar MS (2013) Evaluation of ASCAT based daily gridded winds in the tropical Indian Ocean. *J Atmos Ocean Technol* 30:1371–1381. doi:10.1175/JTECH-D-12-00227.1
- Stommel H (1960) Wind-drift near the equator. *Deep-Sea Res* 6:298–302
- Uppala SM et al (2005) The ERA-40 re-analysis. *Q J R Meteorol Soc* 131:2961–3012. doi:10.1256/qj.04.176
- Vogelzang J, Stoffelen A, Verhoef A, Figa-Saldaña J (2011) On the quality of high-resolution scatterometer winds. *J Geophys Res* 116, C10033. doi:10.1029/2010JC006640
- Wentz FJ, Smith DK, Mears CA, Gentemann CL (2001) Advanced algorithms for QuikSCAT and SeaWinds/AMSR. In: *Geoscience and Remote Sensing Symposium, IEEE 2001 International*, 3; 1079–1081, doi: 10.1109/IGARSS.2001.976752, Institute of Electrical and Electronics Engineers, New York